Electrical activation of insulator-to-metal transition in vanadium dioxide single-crystal nanobeam and their high-frequency switching performances

J.-C. Orlianges, O. Allegret, E.-N. Sirjita, A. Masson, A. Boulle, V. Théry, S. Tardif, J. Micha, A. Crunteanu

Electrical activation of insulator-to-metal transition in vanadium dioxide single-crystal nanobeam and their high-frequency switching performances

J.-C. Orlianges,[1] O. Allegret,[1] E.-N. Sirjita,[1] A. Masson,[2] A. Boulle,[2] V. Théry,[2] S. Tardif,[3] J. S. Micha,[3] and A. Crunteanu[1]

[1)] *XLIM, UMR 7252 CNRS/University of Limoges, 123 Av. A. Thomas 87060 Limoges France*

[2)] *Institut de Recherche sur les Céramiques (IRCER), CNRS UMR 7315, 12 r. Atlantis 87068 Limoges France*

[3)] *CEA-Grenoble/IRIG, 17 rue des Martyrs 38054 Grenoble France*

(*Electronic mail: jean-christophe.orlianges@unilim.fr)

(Dated: 12 July 2024)

We demonstrate the integration of vanadium dioxide single-crystal nanobeams fabricated by modified vapor–liquid–solid method (VLS) as electrical switching elements into a radio-frequency transmission line and evaluate the performances of the overall device in modulating the transmission of the conveyed RF electromagnetic waves. The switching capability of the RF device is based on the metal-insulator transition of VO_2 nanobeams, with on/off electrical switching ratio of 10^4 i.e. resistance modulation from more than $10^6\Omega$ when the wires are in the insulating state to only $\approx 20\Omega$ when they are in the metal-like state. The thermal and electrical activation of the VO_2 wires between the two dissimilar states is resulting RF switching performances characterized by more than $15dB$ change in the transmission coefficient of the device over the $100MHz-24GHz$ frequency domain.

I. INTRODUCTION

Among the strongly correlated electron materials exhibiting insulating to metal transition,[1,2] vanadium dioxide (VO_2) is undoubtedly the one which has attracted the most research interest both from a fundamental point of view,[3] but also for its integration potential into electronic,[4] photonic[5] and neuromorphic devices.[6] The particular attention on VO_2 comes from the large modification of its electrical and optical properties during the onset of the metal-insulator transition (MIT) occurring at relatively low temperatures (insulating behavior below $\approx 340K$ and metal-like characteristics above) and for the possibility to additionally trigger the state change using conveniently implemented electrical or optical stimuli.[5–11] Most of the applications reported in the scientific literature describe the use of the material in the form of thin films. Whether VO_2 thin films are epitaxial or polycrystalline, their insulating to metal transition (IMT) is characterized by the simultaneous coexistence of different phases and its percolative insulator-metal nature.[7,8] These peculiar properties triggered the demonstration of electrical and high frequency devices with interesting performance.[10,11] Thus, due to their broadband electrical response, vanadium dioxide thin films were integrated as localized switching or tuning elements in devices spanning large operational frequency domains, from microwaves and millimeter waves up to terahertz waves.[10–12] Among currently employed deposition techniques for growing high quality VO_2 thin films are pulsed laser deposition,[3,8,13] magnetron sputtering[11,14] or reactive electron-beam evaporation.[15] Chemical vapor deposition (CVD) or Vapor-Liquid-Solid (VLS) techniques were recently applied to fabricate, in a simple way, VO_2 nano / microobjects like wires, plates, beams and nanoparticles which have the particularity of being single-crystalline.[16] This specificity of their crystalline structure makes it possible to overcome the random, percolative domain structures occurring in thin films, hardly compatible with production of reliable and reproducible devices.[17] Initial reports on VO_2 wires or nanobeams integration in electrical devices were centered on top down approaches starting from VO_2 films and their nanometer scale structuring using electron-beam lithography.[18] Still, the obtained VO_2 beams keep the multi-domain granularity of the initial thin films resulting in strain associated with grain boundaries, dislocations or stoichiometry fluctuations.[19]

Vanadium dioxide micro and nanowires fabricated using the bottom-up VLS-CVD method were since thoroughly investigated not only for their peculiar fundamental properties (investigation of the metal-insulator transition and the associated physics at nanoscale in pure, single-crystal objects) but also for their applications as extremely localized temperature or strain sensors,[20,21] photo-and thermoelectric nanoscale switches,[22] solid-state thermal memories[23] or memristors with self-heating capabilities.[24] Since best quality VO_2 films (in terms of the magnitude of their electrical conductivity variation subsequent to the insulator to-metal transition) are obtained on sapphire substrates at relatively high temperatures (superior to $500^\circ C$), this makes their CMOS (complementary metal oxide semiconductors) monolithic integration within high-frequency devices difficult. Instead, VO_2 micro and nanowires can be fabricated by the CVD method on SiO_2 layers (or substrates) and integrated afterward on a plethora of different substrates, including polymer ones.[25] As RF switches are key elements in reconfigurable telecommunications systems or consumer electronics, many efforts have focused lately on emerging technologies based on micro-and nanoscale devices with, potentially, improved performances than current, more conventional solutions based on CMOS or RF-MEMS technologies.[26] In the past, several reports studied the feasibility of using inorganic nanowires[27] or nanoscale memristors based on conductive filaments[28] as active elements for radio frequency and microwaves switches but no studies have been yet reported on VO_2 nanobeams performances at these frequency domains. Here we report for the first time to the best of our knowledge on the evaluation of

high-frequency characteristics of VO_2 nanobeams and the demonstration of simple switching devices in the microwave domain based on the thermal and electrical activation of the metal-insulator transition in vanadium dioxide single-crystal beams.

II. METHODS

A. Nanowires synthesis

The synthesis was performed by a vapor transport method using commercial V_2O_5 powder employed as precursor for the synthesis of VO_2 crystals, as already reported by Guiton et al.[16] Nucleation and growth of nanowires takes place on the surface of a substrate of $Si(100)$ with a thermal oxide layer ($2\mu m$ thick amorphous SiO_2). The substrate and powder were placed in an alumina boat. The part of the boat containing the powder was introduced precisely in the center zone of a high temperature tube furnace. After a primary vacuum step, argon was introduced into the tube at a flow rate of $200sccm$ under a pressure of 2 Torr while the furnace was heated at $850°C$ with a speed rate of $6°C/min$. After a one-hour hold at this temperature, the sample was naturally cooled to room temperature in the same pressure conditions. The local differences in the flow of precursor at the substrate surface lead to an inhomogeneity of the morphology and the density of VO_2 nanostructures on the same sample.[29] As shown in Fig. 1 (a) and (b), synthesis can lead to the formation of nano- and micro-scale objects with shapes ranging from micro/nanowires to microplates.

B. Structural characterization

XRD experiments have been performed on a Bruker D8 Discover diffractometer equipped with a parabolic multilayer mirror, a two-reflection asymmetrically cut $Ge(220)$ monochromator ($Cu\ K_{\alpha 1}$ radiation, $\lambda = 1.5406Å$) as primary optics and linear position sensitive detector. They were performed in a $\theta - 2\theta$ configuration between 15 and 80° with a 0.01° angular resolution.

Micro-diffraction Laue pattern of a VO_2 nanobeam have been obtained at the BM32-IF beamline of the European Synchrotron Radiation Facility (ESRF) using the diffraction experimental setup in which the focused electrons beam has energies in the $5 - 22keV$ range and a spot size of $500x500nm^2$.

C. DC and high-frequency measurements

To study its dc and high-frequency thermal and electrical switching properties, a single VO_2 nanobeam ($14\mu m$ in length, width of $1.5\mu m$ and height of $600nm$) was integrated between the two discontinuous parts ($10\mu m$ apart) of the central signal line of a coplanar waveguide (CPW, microwave transmission line), as shown in Fig. 1(d), where the nanobeam act as a tunable impedance in the CPW. The device designed on the SiO_2/Si substrate has a center signal conductor (S) and two outer ground conductors (G) supporting travelling electromagnetic (EM) waves, with dimensions (width of the signal line and gap between the central line and grounds) adapted to 50Ω. The device was fabricated by conventional photolithography techniques using $500nm$ thick molybdenum (Mo) electrodes obtained by DC magnetron sputtering and patterned by photolithography and wet etching.
The high-frequency performances of the CPW device were evaluated in the transmission mode using a pair of Ground-Signal-Ground (GSG) high-frequency probes (Cascade, with $125mm$ spacing between the G-S-G individual probes) connected to a vector network analyzer (VNA) (ZVA from Rohde & Schwarz).

III. RESULTS AND DISCUSSION

Fig. 1 (c) displays the XRD data recorded for as-grown VO_2 nanowires on SiO_2/Si substrates. In the $\theta - 2\theta$ scan, only 011 reflections from monoclinic VO_2 M1 phase and 400 reflections from Si are observed, which demonstrates that the VO_2 nanostructures grow with the (011) planes parallel to the surface of the sample. These XRD macroscale results were confirmed by structural analysis of individual nanobeams using Laue micro-diffraction measurements, which are showing the presence of both VO_2 M1 (011) and VO_2 M1 (0-11) twinning orientations as illustrated in Fig. 2).

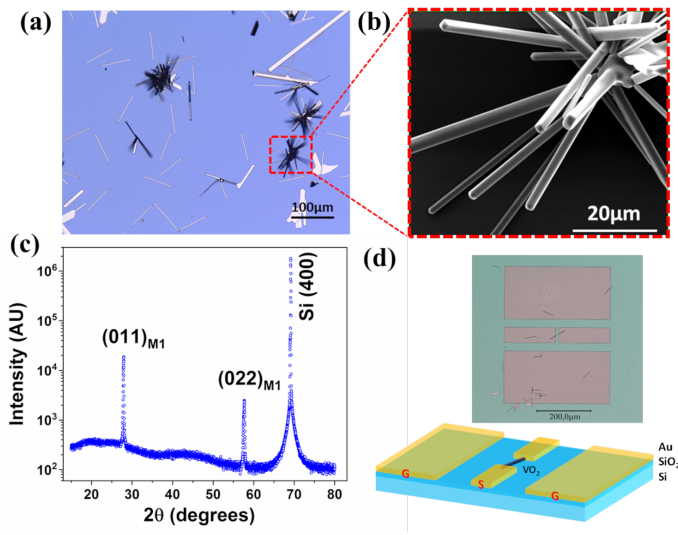

FIG. 1. (a) Optical microscopy image of as grown VO_2 nanostructures (nanowires, nanobeams, microwires…) deposited at $850°C$ on SiO_2/Si substrate (b) SEM micrograph of a cluster of nanowires illustrating their rectangular section (c) X-ray diffraction data of the VO_2 NWs sample (d) 3D sketch and optical microscopy image of the measuring device integrating VO_2 nanobeam

Fig. 3 displays the temperature dependence of electrical resistivity of a VO_2 nanobeam measured using the fabricated device. When the temperature rises, a first jump of resistivity is observed towards $60°C$, corresponding to the transition

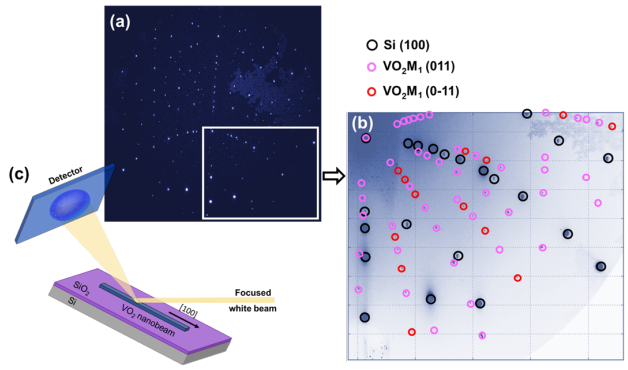

FIG. 2. (a) Micro-diffraction Laue pattern of a VO_2 nanobeam on SiO_2/Si substrate obtained at the BM32-IF beamline of the ESRF (b) Set of diffraction spots from both orientations of M1 VO_2 twins (and from Si substrate) (c) Schematic of the micro diffraction experimental setup in which the focused electrons beam has energies in the $5-22keV$ range and a spot size of $500x500nm^2$

between the M1 and M2 monoclinic insulating states.[30] Then the resistivity gradually decreases until $100°C$ where it drops to the metallic resistivity value of the rutile R phase. For the cooling process, the path is simpler, the material is suddenly transitioning from the metallic to the insulating state M1 at a temperature of $70°C$. The large hysteresis width of the temperature-dependent resistance and the remarkably high insulator to metal transition temperature during heating are attributed to the defect-free, single-crystalline and single domain structure of the measured nanowire.[31]

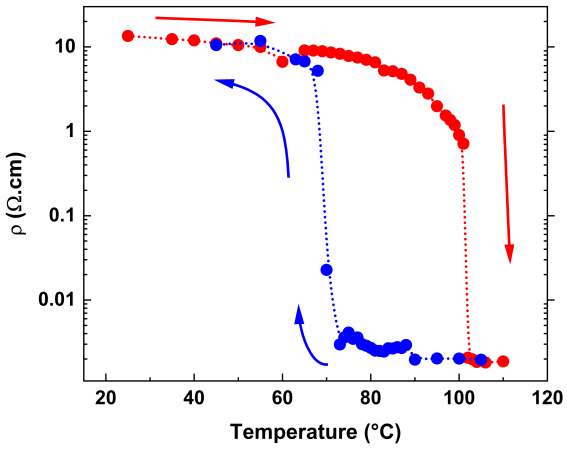

FIG. 3. Resistivity variation with temperature of the VO_2 nanobeam integrated in the CPW device during a heating-cooling cycle between 20 and $110°C$

Fig. 4 (a) and (b) show a typical current-voltage (I-V) curve of the device measured at $50°C$, as the applied bias voltage is increased from 0 to $10V$ then decreased to -10V and then finally brought back to 0V. As illustrated on the inset in the Fig. 4 (a), a $1k\Omega$ resistor is used to limit the current flowing through the nanowire when switching into the metallic state. When the voltage increases beyond a threshold voltage, $V_t = 9V$, we can observe the sudden switching from the insulating state to the metallic state of the vanadium dioxide. Subsequently, when the voltage decreases, the metallic state of the nanowire persists down to a voltage of approximately $1.2V$. This behavior is perfectly symmetrical for applied negative voltages. These I(V) measurements were carried out at different temperatures below the material's transition temperature. From these results, it is possible to estimate the necessary voltage drop on the VO_2 nanobeam (V_{MIT}) for the onset of its insulator-metal transition. Fig. 4 (c) illustrates the strong dependence of this activation voltage on the temperature. The linearity of the power dissipated in the nanowire (proportional to the square of V_{MIT}) as a function of the temperature indicate that the Joule heating mechanism explains the voltage-induced MIT transition.[32,33] Indeed, when the transition is driven by Joule heating, the power P_{MIT} required to induce the activation of the nanowire depends on the temperature according to a relationship of the form:[33]

$$P_{MIT} = \frac{V_{MIT}^2}{R_I(T)} = G_{therm}(T_{MIT} - T) \quad (1)$$

with G_{therm} is the thermal conductance of the overall device, $R_I(T)$ is the resistance of the device for a nanowire in the insulating state at the temperature T and T_{MIT} is the transition temperature.

The high-frequency performances of the CPW device integrating the VO_2 nanobeam were evaluated in the $100MHz - 24GHz$ frequency domain in the transmission mode. The transmission (S_{12} and S_{21}) and reflection (S_{11} and S_{22}) parameters at the two-ports of the symmetrical CPW device ($S_{12} = S_{21}$ and $S_{11} = S_{22}$) were recorded while heating the device through the VO_2 nanobeam transition temperature. Alternatively, the VO_2 material was electrically polarized at fixed, room temperature, by superposing on the RF signal a DC voltage between the two parts of the signal line using DC bias Ts.

The transmission S_{12} parameters of the CPW device are shown on Fig. 5 (a) when thermally cycled between room temperature ($24°C$) and $105°C$, through the insulator-to metal transition temperature of the VO_2 single crystal. At room temperature, the device is significantly blocking the transmission of the RF signal (Off state), with an isolation (attenuation of the transmitted signal) higher than 20 dB through the entire measured frequency domain. As the temperature of the device is increased over $100°C$, the VO_2 beam becomes conductor and allow the RF waves to be transmitted through the coplanar waveguide (On state).

The hysteretic behavior of the transmission coefficient with temperature is highlighted in fig. 5 (b), (c) and (d) for frequencies of $5MHz$, $10GHz$ and $20GHz$ respectively. These hysteresis characteristics are similar to those obtained when measuring the resistance variation of the nanowire with temperature shown in fig. 3.

The transmission losses in the metal-like state of the VO_2 nanobeam (better than 4 dB up to 24 GHz) can be perceived as relatively high, but this can be explained by the impedance mismatch within the gap of the CPW device and the resistance

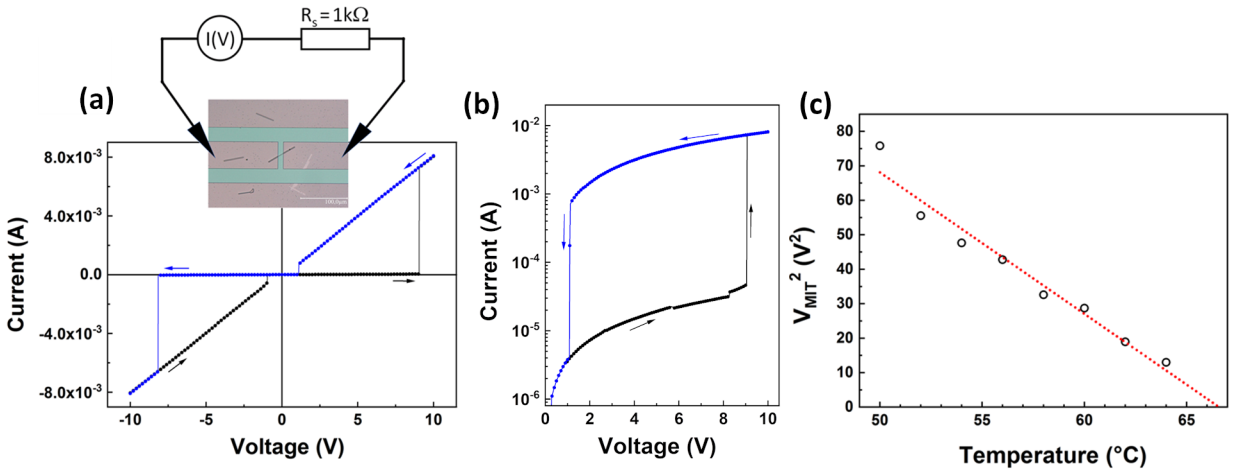

FIG. 4. (a) Current voltage characteristic of the single domain VO_2 wire integrated in the CPW device at $50°C$, illustrating the insulator –to-metal threshold voltage switching at $\approx 9V$ and the hysteretic behavior of the I-V curve; (b) Same graphical representation in logarithm scale for positive voltage values (c)
Plot of V_{MIT}^2 (threshold voltage to induce MIT in the nanobeam) versus the temperature.

in the conductive state of the active VO_2 area, in the order of $2\Omega/\mu m$. These losses can be further reduced to acceptable values (< 1dB) through more adapted CPW designs, by decreasing the distance between the two parts of the RF signal line or by stacking in parallel several VO_2 wires in order to decrease their equivalent linear resistance in the metallic state under $1\Omega/\mu m$. The device can be modeled by a simple electrical circuit consisting of a capacitor (C_{OFF}) in parallel with a high-value resistance (R_{OFF}) when the VO_2 beam is in the insulating state and by a simple resistive impedance with a low value (R_{ON}) when the VO_2 material is in the conducting state.

The high frequency performances of RF switching technologies can be described by their figure of merit, expressed as:

$$FOM = R_{ON} \times C_{OFF} \tag{2}$$

The lower the FOM, the better the RF switching performances of a specific switching device. R_{ON} can be extracted from the experimental insertion loss (IL) data of the device (S_{12} at high temperature, VO_2 in the conductive state), while C_{OFF} can be evaluated from the measured device isolation (S_{12} parameter measured below the transition temperature, when VO_2 is in the insulating state), according to the expressions below:[38]

$$IL\,(dB) = 20\,log\left(1 + \frac{R_{ON}}{2\,Z_0}\right) \tag{3}$$

$$Isolation\,(dB) = 10\,log\left(1 + \left(\frac{1}{2\,Z_0\,\omega\,C_{OFF}}\right)^2\right) \tag{4}$$

Thus, at 24 GHz, we obtain for the single nanobeam VO_2 switching device a $FOM \approx 180fs$. This value is similar or better than the state-of-the art of current semiconductor-based switching technologies.[39]

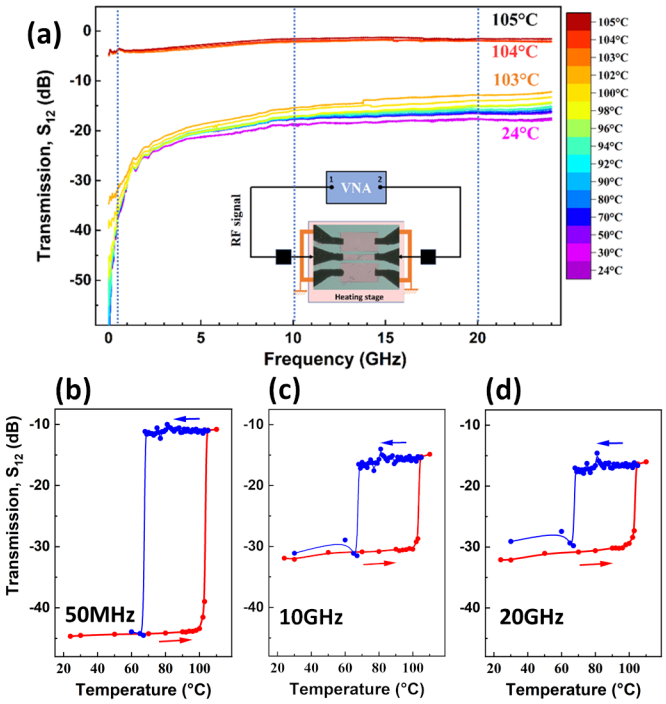

FIG. 5. (a) Transmission (S_{12} parameter) of the CPW device during heating from room temperature to $105°C$ (b), (c) and (d) Evolution of the transmission coefficient as a function of temperature for a rise (in red) and a decrease (in blue) at frequencies of 5MHz, 10GHz and 20GHz respectively.

In order to electrically actuate the VO_2 nanobeam within the CPW, we connected the device (via bias Ts) to a simple electrical polarization circuit (presented in the inset of Fig. 6) allowing to apply a voltage between the two segments of the

TABLE I. List of VO_2-based RF switch specifications extracted from relevant reports in the literature

Reference	Activation mode	Switching amplitude at 20GHz	VO_2 synthesis method	Substrate
Li et al.[34]	Thermal activation	11-12dB	Screen printing of VO_2 ink	Kapton
Yang et al.[35]	Thermal activation	12-13dB	Screen printing of VO_2 ink	sapphire
Crunteanu et al.[9]	Thermal and electrical activations	20dB	e-beam evaporation	sapphire
Jiang et al.[36]	Thermal activation	27dB	RF sputtering	SiN/SiO_2/Alumina
Lee et al.[37]	Thermal activation	13-15dB	Pulsed laser deposition	$SnO_2/TiO_2(001)$
This work	Thermal and electrical activations	15dB	VLS nanowires	SiO_2/Si

CPW signal line separated by the VO_2 beam.

The measured transmission S_{12}-parameters at $58°C$ of the device submitted to a periodic square-type voltage signal ($5V$ amplitude, $2Hz$) is shown on Fig.6. As the material is changing between the two states following the electrical activation, the impedance of the VO_2 beam is rapidly and periodically modified between its extreme values, reflected in the periodic modulation of the S_{12} parameter. The switching dynamics of the device is relatively important, keeping in mind that the active part of the material is composed of only a $10\mu m$ long VO_2 nanobeam. As in the case of thermal activation, this dynamics can be further improved by using shorter VO_2 beams and decreasing the gap between the two parts of the signal line or by integrating several beams in parallel within the CPW gap for decreasing the overall R_{ON} of the device. We compare, in Table I, the performances of our device with similar RF devices integrating VO_2 thin films, extracted from relevant reports in the literature. As mentioned above, even if the design of our proposed device can be further improved to consider the limited size of the VO_2 nanowire, its switching performances compare rather well with similar VO_2-based thin films RF switches.

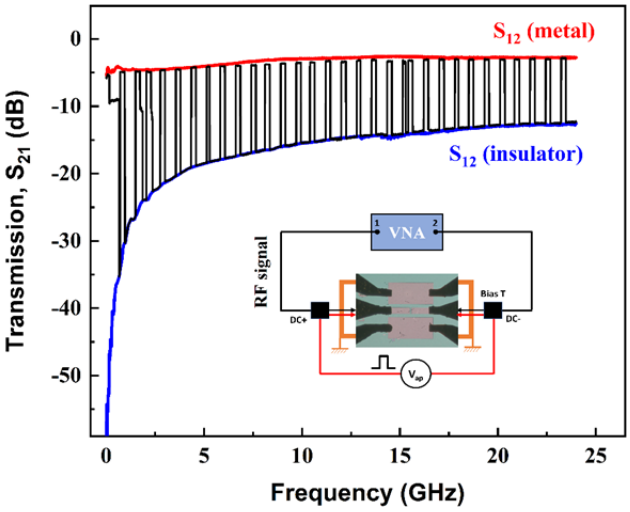

FIG. 6. Dynamic variation of the S_{21} parameter (transmission of the CPW line) for the series VO_2-wire switch (inset) submitted to a square-shaped electrical activation waveform periodically activating the IMT in the VO_2 material

IV. CONCLUSION

In conclusion, we presented the proof of concept and experimental demonstration of microwave switching using thermal and electrical activation of the insulator-to-metal transition in VO_2 single-crystal beams. Compared with VO_2 films, vanadium dioxide nanobeams have higher insulator-to-metal activation temperatures implying more stable electrical performances for larger temperature domains, up to $100°C$. They present convenient reversible and repetitive thermal and electrical switching behavior with more than 15 dB switching amplitude between the two states in the $100MHz - 24GHz$ domain. While the performances of the devices presented here can be further improved by conveniently adjusting their topologies (beam parallelization, dimensions), the demonstration of RF signals switching using VO_2 nanobeams initiates interesting opportunities for micro and nanoscale microwave devices for efficient switching and modulation of electromagnetic signals in the microwaves and millimeter waves domains.

ACKNOWLEDGMENTS

This work was financially supported by the Agence Nationale de la Recherche (ANR) under grant no. ANR-22-CE24-0016, CIRANO project.

DATA AVAILABILITY STATEMENT

The data that support the findings of this study are available from the corresponding author upon reasonable request.

[1] S. D. Ha and S. Ramanathan, "Adaptive oxide electronics: A review," Journal of applied physics **110** (2011).
[2] Y. Yu, Y. Cui, J. He, W. Mao, and J. Chen, "Metal-to-insulator transitions in 3d-band correlated oxides containing Fe compositions," International Journal of Minerals, Metallurgy and Materials **31**, 48–59 (2024).
[3] N. B. Aetukuri, A. X. Gray, M. Drouard, M. Cossale, L. Gao, A. H. Reid, R. Kukreja, H. Ohldag, C. A. Jenkins, E. Arenholz, *et al.*, "Control of the metal–insulator transition in vanadium dioxide by modifying orbital occupancy," Nature Physics **9**, 661–666 (2013).
[4] Y. Zhou, X. Chen, C. Ko, Z. Yang, C. Mouli, and S. Ramanathan, "Voltage-triggered ultrafast phase transition in vanadium dioxide switches," IEEE Electron Device Letters **34**, 220–222 (2013).
[5] R. M. Briggs, I. M. Pryce, and H. A. Atwater, "Compact silicon photonic waveguide modulator based on the vanadium dioxide metal-insulator phase transition," Optics express **18**, 11192–11201 (2010).

[6] W. Yi, K. K. Tsang, S. K. Lam, X. Bai, J. A. Crowell, and E. A. Flores, "Biological plausibility and stochasticity in scalable VO_2 active memristor neurons," Nature communications **9**, 4661 (2018).

[7] M. M. Qazilbash, M. Brehm, B.-G. Chae, P.-C. Ho, G. O. Andreev, B.-J. Kim, S. J. Yun, A. Balatsky, M. Maple, F. Keilmann, *et al.*, "Mott transition in VO_2 revealed by infrared spectroscopy and nano-imaging," Science **318**, 1750–1753 (2007).

[8] G. J. Kovács, D. Bürger, I. Skorupa, H. Reuther, R. Heller, and H. Schmidt, "Effect of the substrate on the insulator–metal transition of vanadium dioxide films," Journal of Applied Physics **109** (2011).

[9] A. Crunteanu, J. Givernaud, J. Leroy, D. Mardivirin, C. Champeaux, J.-C. Orlianges, A. Catherinot, and P. Blondy, "Voltage-and current-activated metal–insulator transition in VO_2-based electrical switches: a lifetime operation analysis," Science and technology of advanced materials (2010).

[10] S. D. Ha, Y. Zhou, A. E. Duwel, D. W. White, and S. Ramanathan, "Quick switch: Strongly correlated electronic phase transition systems for cutting-edge microwave devices," IEEE Microwave Magazine **15**, 32–44 (2014).

[11] C. Hillman, P. Stupar, J. Hacker, Z. Griffith, M. Field, and M. Rodwell, "An ultra-low loss millimeter-wave solid state switch technology based on the metal-insulator-transition of vanadium dioxide," in *2014 IEEE MTT-S International Microwave Symposium (IMS2014)* (IEEE, 2014) pp. 1–4.

[12] E. P. Parrott, C. Han, F. Yan, G. Humbert, A. Bessaudou, A. Crunteanu, and E. Pickwell-MacPherson, "Vanadium dioxide devices for terahertz wave modulation: a study of wire grid structures," Nanotechnology **27**, 205206 (2016).

[13] J.-C. Orlianges, J. Leroy, A. Crunteanu, R. Mayet, P. Carles, and C. Champeaux, "Electrical and optical properties of vanadium dioxide containing gold nanoparticles deposited by pulsed laser deposition," Applied Physics Letters **101** (2012).

[14] P. J. P. Jin and S. T. S. Tanemura, "Formation and thermochromism of VO_2 films deposited by rf magnetron sputtering at low substrate temperature," Japanese journal of applied physics **33**, 1478 (1994).

[15] J. Leroy, A. Bessaudou, F. Cosset, and A. Crunteanu, "Structural, electrical and optical properties of thermochromic VO_2 thin films obtained by reactive electron beam evaporation," Thin Solid Films **520**, 4823–4825 (2012).

[16] B. S. Guiton, Q. Gu, A. L. Prieto, M. S. Gudiksen, and H. Park, "Single-crystalline vanadium dioxide nanowires with rectangular cross sections," Journal of the American Chemical Society **127**, 498–499 (2005).

[17] S. Sengupta, K. Wang, K. Liu, A. K. Bhat, S. Dhara, J. Wu, and M. M. Deshmukh, "Field-effect modulation of conductance in VO_2 nanobeam transistors with HfO_2 as the gate dielectric," Applied Physics Letters **99** (2011).

[18] J. Jeong, Z. Yong, A. Joushaghani, A. Tsukernik, S. Paradis, D. Alain, and J. K. Poon, "Current induced polycrystalline-to-crystalline transformation in vanadium dioxide nanowires," Scientific reports **6**, 37296 (2016).

[19] C. Cheng, K. Liu, B. Xiang, J. Suh, and J. Wu, "Ultra-long, free-standing, single-crystalline vanadium dioxide micro/nanowires grown by simple thermal evaporation," Applied Physics Letters **100** (2012).

[20] H. Guo, K. Chen, Y. Oh, K. Wang, C. Dejoie, S. Syed Asif, O. Warren, Z. Shan, J. Wu, and A. Minor, "Mechanics and dynamics of the strain-induced m1-m2 structural phase transition in individual VO_2 nanowires," Nano letters **11**, 3207–3213 (2011).

[21] H. Guo, M. Khan, C. Cheng, W. Fan, C. Dames, J. Wu, and A. Minor, "Vanadium dioxide nanowire-based microthermometer for quantitative evaluation of electron beam heating," Nature communications **5**, 4986 (2014).

[22] B. Varghese, R. Tamang, E. S. Tok, S. G. Mhaisalkar, and C. H. Sow, "Photothermoelectric effects in localized photocurrent of individual VO_2 nanowires," The Journal of Physical Chemistry C **114**, 15149–15156 (2010).

[23] R. Xie, C. T. Bui, B. Varghese, Q. Zhang, C. H. Sow, B. Li, and J. T. Thong, "An electrically tuned solid-state thermal memory based on metal–insulator transition of single-crystalline VO_2 nanobeams," Advanced Functional Materials **21**, 1602–1607 (2011).

[24] S.-H. Bae, S. Lee, H. Koo, L. Lin, B. H. Jo, C. Park, and Z. L. Wang, "The memristive properties of a single VO_2 nanowire with switching controlled by self-heating," Advanced Materials **25**, 5098–5103 (2013).

[25] B. Hu, Y. Zhang, W. Chen, C. Xu, and Z. L. Wang, "Self-heating and external strain coupling induced phase transition of VO_2 nanobeam as single domain switch," Advanced Materials **23**, 3536 (2011).

[26] G. M. Rebeiz, *RF MEMS: theory, design, and technology* (John Wiley & Sons, 2004).

[27] B. Mirkhaydarov, H. Votsi, A. Sahu, P. Caroff, P. R. Young, V. Stolojan, S. G. King, C. C. Ng, V. Devabhaktuni, H. H. Tan, *et al.*, "Solution-processed InAs nanowire transistors as microwave switches," Advanced Electronic Materials **5**, 1800323 (2019).

[28] S. Pi, M. Ghadiri-Sadrabadi, J. C. Bardin, and Q. Xia, "Nanoscale memristive radiofrequency switches," Nature communications **6**, 7519 (2015).

[29] E. Strelcov, A. V. Davydov, U. Lanke, C. Watts, and A. Kolmakov, "In situ monitoring of the growth, intermediate phase transformations and templating of single crystal VO_2 nanowires and nanoplatelets," ACS nano **5**, 3373–3384 (2011).

[30] J. Cao, Y. Gu, W. Fan, L.-Q. Chen, D. Ogletree, K. Chen, N. Tamura, M. Kunz, C. Barrett, J. Seidel, *et al.*, "Extended mapping and exploration of the vanadium dioxide stress-temperature phase diagram," Nano letters **10**, 2667–2673 (2010).

[31] J. Wei, Z. Wang, W. Chen, and D. H. Cobden, "New aspects of the metal–insulator transition in single-domain vanadium dioxide nanobeams," Nature nanotechnology **4**, 420–424 (2009).

[32] J. Yoon, G. Lee, C. Park, B. S. Mun, and H. Ju, "Investigation of length-dependent characteristics of the voltage-induced metal insulator transition in VO_2 film devices," Applied Physics Letters **105** (2014).

[33] I. P. Radu, B. Govoreanu, S. Mertens, X. Shi, M. Cantoro, M. Schaekers, M. Jurczak, S. De Gendt, A. Stesmans, J. Kittl, *et al.*, "Switching mechanism in two-terminal vanadium dioxide devices," Nanotechnology **26**, 165202 (2015).

[34] W. Li, M. Vaseem, S. Yang, and A. Shamim, "Flexible and reconfigurable radio frequency electronics realized by high-throughput screen printing of vanadium dioxide switches," Microsystems & nanoengineering **6**, 77 (2020).

[35] S. Yang, M. Vaseem, and A. Shamim, "Fully inkjet-printed VO_2-based radio-frequency switches for flexible reconfigurable components," Advanced Materials Technologies **4**, 1800276 (2019).

[36] J. Jiang, G. Chugunov, and R. R. Mansour, "Fabrication and characterization of VO_2-based series and parallel rf switches," in *2017 IEEE MTT-S International Microwave Symposium (IMS)* (IEEE, 2017) pp. 278–280.

[37] J. Lee, D. Lee, S. J. Cho, J.-H. Seo, D. Liu, C.-B. Eom, and Z. Ma, "Epitaxial VO_2 thin film-based radio-frequency switches with thermal activation," Applied Physics Letters **111** (2017).

[38] D. M. Pozar, *Microwave engineering* (John wiley & sons, 2011).

[39] F. Gianesello, A. Monroy, V. Vialla, E. Canderle, G. Bertrand, M. Buczko, M. Coly, J. Nowakowski, N. Revil, L. Rolland, *et al.*, "Highly linear and sub 120 fs ron× coff 130nm rf soi technology targeting 5g carrier aggregation rf switches and fem soc," in *2016 IEEE 16th Topical Meeting on Silicon Monolithic Integrated Circuits in RF Systems (SiRF)* (IEEE, 2016) pp. 9–12.